Awschalom, *Science* **262**, 1249 (1993); J. Shi, S. Gider, K. Babcock, D. D. Awschalom, *ibid.* **271**, 937 (1996).
11. S. Y. Chou, P. R. Krauss, L. Kong, *J. Appl. Phys.* **79**, 6101 (1996).
12. J. Dooley and M. De Graef, *Ultramicroscopy* **67**, 113 (1997); M. De Graef, N. T. Nuhfer, M. R. McCartney, *J. Microsc.*, in press.
13. H. W. Fuller and M. E. Hale, *J. Microsc.* **31**, 238 (1960).
14. A. Hütten, J. Bernardi, C. Nelson, G. Thomas, *Phys. Status Solidi A* **150**, 171 (1995).
15. C. Salling, S. Schultz, I. McFayden, M. Ozaki, *IEEE Trans. Magn.* **27**, 5184 (1991); G. A. Gibson, J. F. Smyth, S. Schultz, D. P. Kern, *ibid.*, p. 5187; M. Lederman, G. A. Gibson, S. Schultz, *J. Appl. Phys.* **73**, 6961 (1993).
16. H. W. Fuller and M. E. Hale, *J. Appl. Phys.* **31**, 1699 (1960).
17. S. A. Majetich and E. M. Kirkpatrick, *IEEE Trans. Magn.* **33**, 3721 (1997); S. A. Majetich *et al.*, *Nanostruct. Mater.* **9**, 291 (1997).
18. Based on the size criterion for superparamagnetic behavior given in (*2*), 10-nm particles of Fe_3O_4 are expected to be superparamagnetic at room temperature. As found experimentally in J. Zhang, C. Boyd, and W. Luo [*Phys. Rev. Lett.* **77**, 390 (1996)], when a ferrofluid is diluted so that the particle separation is large (as in the TEM samples we studied), Néel relaxation or superparamagnetic behavior is observed.
19. J. H. Scott and S. A. Majetich, *Phys. Rev. B* **52**, 12564 (1995); Z. Turgut, J. H. Scott, M. Q. Huang, S. A. Majetich, M. E. McHenry, *J. Appl. Phys.* **83**, 6468 (1998).
20. B. D. Cullity, *Introduction to Magnetic Materials* (Addison-Wesley, Reading, MA, 1972), p. 413.
21. M. Born and E. Wolf, *Principles of Optics* (Pergamon, Oxford, 1970), p. 420.
22. Y. Aharonov and D. Bohm, *Phys. Rev.* **115**, 485 (1959).
23. D. Wohlleben, *J. Appl. Phys.* **38**, 3341 (1967).
24. Z. L. Wang, *Adv. Mater.* **10**, 13 (1998).
25. J. D. Jackson, *Classical Electrodynamics* (Wiley, New York, 1975), pp. 178 and 196–197.
26. R. A. McCurrie, *Ferromagnetic Materials: Structure and Properties* (Academic Press, New York, 1994), p. 142.
27. R. H. Kodama, A. E. Berkowitz, E. J. McNiff Jr., S. Foner, *Phys. Rev. Lett.* **77**, 394 (1996).
28. C. W. Chen, *Magnetism and Metallurgy of Soft Magnetic Materials* (Dover, New York, 1986), p. 211.
29. F. Pfeifer and C. Radeloff, *J. Magn. Magn. Mater.* **19**, 190 (1980).
30. We thank J. Suhan for microtomy sectioning and J. H. Scott for helpful discussions. S.A.M. thanks NSF for financial support (awards DMR-9285308 and DMR-9500313).

16 December 1998; accepted 17 February 1999

A Steric Mechanism for Inhibition of CO Binding to Heme Proteins

Galina S. Kachalova, Alexander N. Popov,* Hans D. Bartunik†

The crystal structures of myoglobin in the deoxy- and carbon monoxide–ligated states at a resolution of 1.15 angstroms show that carbon monoxide binding at ambient temperatures requires concerted motions of the heme, the iron, and helices E and F for relief of steric inhibition. These steps constitute the main mechanism by which heme proteins lower the affinity of the heme group for the toxic ligand carbon monoxide.

The structural basis of the discrimination between O_2 and the toxic ligand CO by heme proteins has been the subject of many experimental and theoretical investigations (*1*). Aside from their role in respiration, CO ligands may act as regulators of cell and organ function (*2*). In addition to environmental sources, CO is produced endogenously in the breakdown of heme. The binding affinity of CO to heme proteins is much lower in comparison to that of porphyrin complexes. The textbook explanation of this difference is centered on the Fe-C-O binding geometry. Whereas this geometry is approximately linear in CO porphyrin complexes (*3, 4*), previously reported x-ray and neutron crystal structures of CO-ligated myoglobin (MbCO) show bent binding geometries with substantial deviations from linearity (*5*). In attempts to interpret these structural data and many infrared (IR) measurements, a number of models have been suggested in which bending of the Fe-CO unit is explained in terms of short-range interactions between the ligand and the distal His of the protein matrix. It was proposed that steric repulsion (*6*), electrostatic interactions between the distal His side chain and the ligand involving strong back-bonding in the Fe-CO unit (*7, 8*), or a non-equilibrium orientation of the proximal His (*9*) may prevent the CO from binding in a linear conformation. However, recent results from IR polarization (*10–12*), Fourier transform IR spectroscopy (*13*), and a joint analysis of nuclear magnetic resonance, Fe^{57} Mössbauer, and IR spectroscopic data (*14*) suggested a nearly linear geometry as the most likely conformation. These results and the large variability in the three-dimensional (3D) structural models raised severe doubts as to the accuracy of the previous crystal structure analyses.

We report the results of x-ray crystallographic studies of native sperm-whale myoglobin at ultrahigh resolution. Essentially unrestrained refinement (Table 1) at a resolution of 1.15 Å of the $P2_1$ crystal structures of deoxy myoglobin (deoxyMb), MbCO, and aquo-met myoglobin (metMb) at pH 6 provided a very high accuracy (average error of 0.03 Å in the positions of main-chain atoms). The structural models differ substantially from the previous crystal structures, in particular with respect to the ligand binding geometry and to the interactions between the ligand and residues inside the distal pocket. Some of these structural differences can be explained by heterogeneities in the ligation states that were not identified in previous crystal structures because of the lower resolution. A comparison of our MbCO and deoxyMb structures provided the basis for analyzing the structural mechanism of CO inhibition. The diffraction studies have been undertaken at room temperature in order to approach physiological conditions as closely as possible.

The MbCO crystal structure shows the individual atoms of the bound CO with full occupancy in a well-resolved electron density (Fig. 1). The ligand adopts a single conformation. The Fe-C-O binding geometry is nearly linear (Fig. 1 and Table 2); the angular deviation θ of the Fe-CO unit from linearity is 7.4° (1.9°) (numbers in parentheses are standard errors of the last digit or digits). The Fe-C bond is tilted by an angle $\tau = 4.7°$ (0.9°) with respect to the normal to the nitrogen plane that is formed by the four pyrrole N ligands that surround the heme Fe in a nearly perfect square planar symmetry. Our results confirm theoretical estimates by Ray *et al.* (*8*) and remove the controversy between spectroscopy and previous crystal structures, which were interpreted in terms of more strongly inclined binding geometries and disordered CO sites (*5*). The angular geometry of the Fe-CO unit in the crystal structure is in close agreement with recent spectroscopic data for MbCO in solution (*10–12, 14*) and in the $P2_1$ and $P2_12_12_1$ crystal forms (*10–12*). When comparing the structures of MbCO and unencumbered porphyrin complexes, we found that the deviation of the Fe-CO unit from linearity (Table 2) is slightly stronger, by a few degrees, in MbCO. This additional distortion involves energies that are too small to explain the reduced binding affinity of CO to Mb (*10–12*). The Fe-C and the C-O bond lengths agree within the experimental errors (Table 2).

The internal structure of the heme is rather insensitive to the binding of CO. The tilt angles between the individual pyrrole rings and the nitrogen plane are nearly the same in MbCO

Max-Planck-Arbeitsgruppen für Strukturelle Molekularbiologie, Arbeitsgruppe Proteindynamik, Notkestraße 85, 22603 Hamburg, Germany.

*Present address: European Molecular Biology Laboratory Outstation, Notkestraße 85, 22603 Hamburg, Germany.

†To whom correspondence should be addressed. E-mail: bartunik@mpghdb.desy.de

as in Fe(TPP)(CO)py (TPP, 5,10,15,20-tetraphenylporphyrin dianion; py, pyridine) (Table 3), except for a stronger out-of-plane inclination of the C pyrrole ring in MbCO. The tilt angles between the nitrogen plane and each of the pyrrole rings increase by 2°. In addition, the square formed by the four pyrrole N ligands of the Fe slightly contracts (from 4.07 to 4.00 Å, measured along the diagonals). The changes are due to a movement of the heme Fe from its location on the proximal side in deoxyMb (distance Δ_{Mb} = 0.290 Å from the nitrogen plane) into the nitrogen plane of MbCO (Δ_{MbCO} = 0.015 Å on the distal side). This displacement of the Fe is substantially smaller than that previously described (*5, 15*). The covalent bond length between Fe and the Nε_2 of the proximal His, His^{93} (also residue 8 of helix F, or F8), shortens slightly (from 2.15 to 2.12 Å) upon binding of CO. The orientation of the imidazole ring, which is stabilized by the H-bonding interaction between Nδ_1 and Leu^{89} O, remains essentially unchanged. There is no evidence for a nonequilibrium orientation of the proximal His.

The orientation of the CO ligand in MbCO is defined by repulsive interactions of the CO oxygen with two highly conserved distal residues, His^{64} (E7) and Val^{68} (E11) (Fig. 1 and Table 2). The Val^{68} Cγ_2 atom is at a rather short distance (3.13 Å) from the CO oxygen; this finding explains why mutations at E11 to residues with more bulky side chains were found (*1*) to cause steric hindrance to the binding of CO to Mb. Val^{68} hinders the access of the CO to the sixth coordination site of the heme Fe as long as the conformation of the protein matrix and the orientation of the heme remain as in deoxyMb. This conclusion is derived from an alignment of the 3D structures of deoxyMb and MbCO on a common rigid domain that essentially consists of helices A, B, D, and H [root-mean-square deviation (rmsd) of 0.09 Å of the main-chain atoms]. When a CO molecule is inserted in the structural model of deoxyMb so that its position and orientation relative to the nitrogen plane of the heme is the same as in MbCO, the CO oxygen is only 2.7 Å from Cγ_2 of Val^{68}. The steric hindrance is removed by correlated motions that the heme and part of the protein matrix undergo with respect to the rigid domain of the globin. Upon ligand binding, the E and F helices, which hold the heme like a pair of tweezers, undergo rigid-body movements. In a plane that contains F and is roughly perpendicular to the nitrogen plane of the heme, the "V" formed by both helices translates and rotates as a rigid unit. The translation by 0.12 Å occurs in the direction from pyrroles B to D along the interface between the EF corner of the heme pocket and helix H in the rigid domain of the globin, without substantially affecting the H-bond His^{82} (EF5) Nε_2–Asp^{141} (H18) Oδ_2. The "V" rotates by an angle δ = 0.9° around a pivot point that is located near Lys^{79} in the EF corner. The displacement of the Fe in this projection can be described with the same rotation and translation parameters; that is, the Fe and the two helices keep their relative orientations. The rotations of E and F displace the backbone segments near the distal and proximal histidines by amplitudes (~0.3 to 0.4 Å) that are small but highly significant; they exceed the average error in the atomic coordinates by more than one order of magnitude. In a different projection that is approximately parallel to the nitrogen plane, helix F and the heme, together with the Fe, undergo a joint rotation (by ε_F = 0.9°) around the same pivot in the EF corner, whereas helix E rotates by about the same angle (ε_E) in the opposite direction. Thus, E and F exhibit a scissorlike motion in this projection, with an angular amplitude of 1.7° in relation to each other. The movements of the E and F helices in relation to the neighboring helices cause a reorientation of the hydrophobic lining of the heme pocket. Whereas Val^{68} (E11) and Leu^{89} (F4) near pyrrole ring A move in the same direction as the heme Fe, the residues Ile^{99} (FG5), Leu^{104} (G5), and Ile^{107} (G8), which form a hydrophobic clamp around pyrrole ring C, move in the opposite direction because of a change in the conformation of the FG corner. The orientations of other hydrophobic residues, including Phe^{138} (H15) and Phe^{43} (CD1), that interact with the heme near pyrrole B or D are not affected. The motions in the hydrophobic environment of the heme are associated with a tilt of the nitrogen plane by 4.0° around NB-ND and a translation by 0.19 Å in the direction from NA to NC. The combined shift and tilt of the heme can be described by a single rotational movement

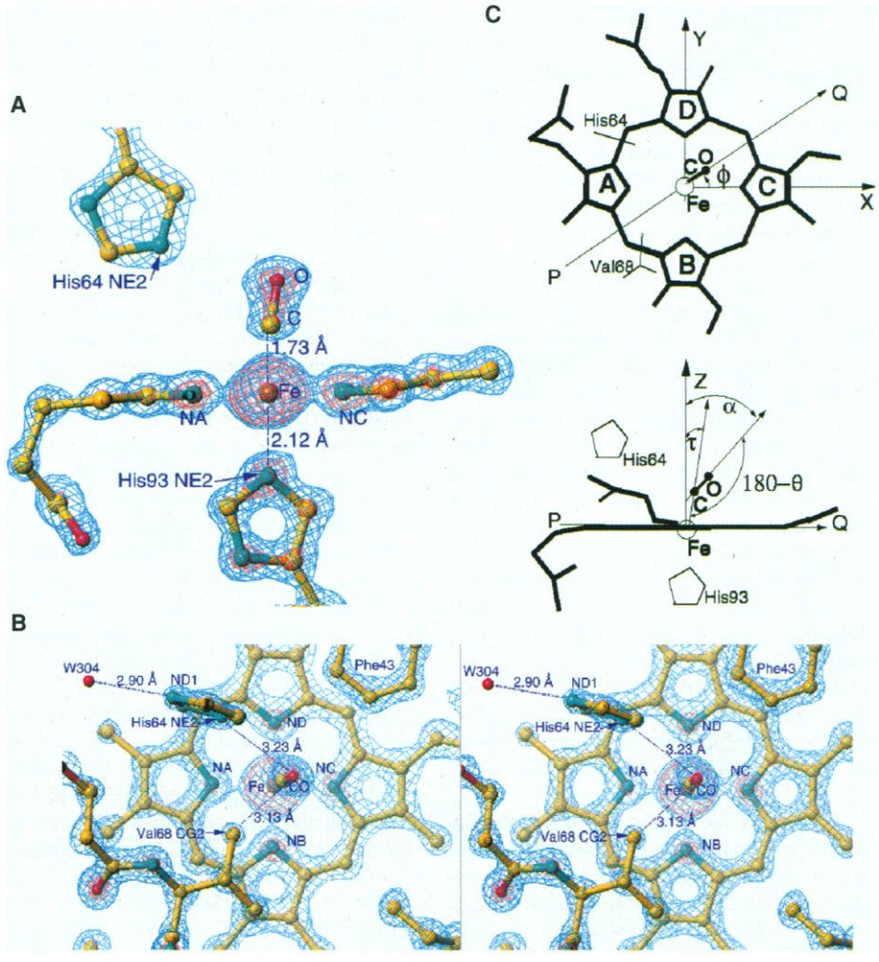

Fig. 1. CO binding site and environment in MbCO. (**A**) Side view. The $2|F_o| - |F_c|$ map is contoured at 2.4σ (blue) and 4.0σ (red) (σ, standard deviation). (**B**) Stereoview from the distal side. Contours are at 2.8σ (blue) and 5.0σ (red). (**C**) Polar angles ϕ and α (= $\theta + \tau$) describing the Fe-C and C-O orientations in MbCO. The azimuthal angles ϕ_{FeC} = 33.4° and ϕ_{CO} = 24.3° were measured from the NA-NC axis. The estimate of the errors in the tilt angle τ = 4.7° ± 0.9° and the bending angle θ = 7.4° ± 1.9° is based on the uncertainties at a 1σ level in the refined atomic coordinates. (A) and (B) were prepared with TURBO FRODO (*32*).

around an axis that is parallel to NB-ND and runs through the proximal His side chain. The tilt of the heme and the motions of helices E and F cooperate in the formation of the active binding site of the CO in MbCO (Fig. 2).

The high flexibility of the His^{64} side chain in Mb suggests a different structural role of this residue. The repulsive interaction with the bound CO ligand causes the imidazole to swing away from the active binding site in a direction that is parallel to the NC-NA axis. The amplitude of this swinging motion is substantially greater in MbCO than in deoxyMb or in metMb; the imidazole remains, however, inside the heme pocket in all three structures at pH 6 (*16*). His^{64} in MbCO is well ordered; its side chain adopts a single conformation with full occupancy in which $N\varepsilon_2$ of the imidazole points toward the CO oxygen. There is no or only a very weak H bond between the $N\varepsilon_2$ and the CO oxygen (distance of 3.23 Å). This finding contradicts a previous assumption, based on molecular dynamics (MD) calculations, that $N\varepsilon_2$ is engaged in a long-lived H-bonding interaction with the CO (*17*). The short C-O bond length (1.12 Å) in the MbCO structure is consistent with a formal bond order of three (*18*) and indicates that the back donation of Fe d_π electrons to the π^* orbitals of CO is inhibited, which can be expected when the lone pair of $N\varepsilon_2$ points to the CO oxygen (*8*). In deoxyMb, the His^{64} side chain occupies two alternate locations, exhibiting comparable populations, which differ in their distance from the sixth coordination site of the heme Fe. The tilt of the heme and the reorientational motions in the protein matrix accompanying ligation with CO enhance these distances. However, different from the case of Val^{68}, an additional displacement of the imidazole (by 0.9 and 1.4 Å for the two conformers, respectively) away from the CO ligand is needed in order to reach a similar orientation as in MbCO. The direction and amplitude of this displacement suggest that it may be related to a translocation of the ligand from a docking site to the active binding site. Two possible CO docking sites in MbCO have been located above NC at 20 to 40 K (*19–21*). An alignment of the low-temperature x-ray structure of photodissociated Mb by Schlichting *et al.* (*19*) on the present deoxyMb structure shows that this possible docking site, which is nearly identical to the location of the "deoxy water" (W378), is ~1.6 Å from the active binding site. The corresponding distance for the docking site, reported by Teng *et al.* (*20*), is ~1.0 Å. The results of spectroscopic studies (*22*) and MD calculations (*23*) suggest a close similarity in the proposed CO docking sites at low and at ambient temperatures.

There is no direct structural evidence for a possible involvement of the distal His in the access of CO to the distal pocket. In particular, our crystal structures at pH 6 do not show any evidence for an outward movement of the His side chain (*16*), which has been suggested to open a channel between the solvent region and the heme pocket (*5*). We cannot exclude the possibility that the His^{64} imidazole infrequently swings out of the heme pocket to a site with low occupancy (<5%). In fact, His^{64} appears to play a role in the passage of water from the solvent region into the distal pocket. Whereas MbCO does not contain any water in the distal pocket, deoxyMb has a half-populated water molecule (W378) near the sixth coordination site of the Fe. W378 is H bonded to one conformer of His^{64} (His^{64}-I) (distance of 2.77 Å between $N\varepsilon_2$ and the water oxygen), which has a

Table 1. Data collection and refinement statistics. X-ray diffraction data were measured at room temperature on the wiggler beamline BW6 at the Deutsches Elektronen-Synchrotron (Hamburg) using the rotation method and a MAR345 imaging plate scanner. Values in parentheses are for the highest resolution shell, 1.20 to 1.15 Å (for metMb, 1.22 to 1.20 Å). The data were processed, merged, and scaled with DENZO/SCALEPACK (*28*). The structures were refined with SHELXL-97 (*29*) using anisotropic displacement parameters and H atoms at calculated positions. All reflections were included in the refinement procedure. $R_{merge} = \Sigma_{hkl}\Sigma_i|I_i - \langle I\rangle|/\Sigma_{hkl}\Sigma_i\langle I\rangle$, where I_i is an intensity I for the ith measurement of a reflection with indices hkl and $\langle I\rangle$ is the weighted mean of all measurements of I. $R_{cryst} = [\Sigma_{hkl}||F_o(hkl)| - |F_c(hkl)||]/\Sigma_{hkl}|F_o(hkl)|$, where F_o and F_c are the observed and calculated structure factors, respectively. R_{free} is the crystallographic R value calculated with 5% of the data excluded from the refinement calculation. The refined model of metMb was used as an initial model for deoxyMb and MbCO. Estimates of the averaged standard deviations (Esd) were obtained from SHELXL-97 with the Cruickshank formula (*30*). The porphyrin atoms were refined with distance restraints only. The positions of the Fe and of the atoms of the CO ligand were refined without any restraints. The program O (*31*) was used for model building. As an independent check of the homogeneity in the ligandation states, the extent of ligation was studied for each preparation by visible absorption spectroscopy; for this purpose, we dissolved, under anaerobic conditions, crystals that were prepared simultaneously under identical conditions and were of a similar size as those used for x-ray data collection. σ, standard deviation; deg, degrees; dashes indicate no data available.

Item	deoxyMb	MbCO	metMb
	Data collection		
Space group	$P2_1$	$P2_1$	$P2_1$
Unit cell			
a (Å)	35.15	34.91	34.83
b (Å)	31.04	31.04	30.92
c (Å)	64.59	64.73	64.57
β (deg)	105.58	105.53	105.50
Resolution (Å)	1.15 to 12.0	1.15 to 12.0	1.20 to 12.0
Measured reflections	175,253	202,454	564,343
$\langle I\rangle/\langle\sigma(I)\rangle$	19.9 (2.7)	23.8 (3.4)	30.4 (6.6)
Unique reflections	41,190	46,002	41,485
Completeness (%)	85.9 (66.1)	96.3 (95.3)	99.4 (100.0)
R_{merge} (%)	6.2 (36.2)	5.2 (28.2)	4.8 (28.2)
	Refinement		
Parameters/reflections	14,105/41,190	13,701/46,002	14,814/41,485
R_{cryst} for all F_o (%)	11.4	12.4	9.0
R_{cryst} for $F_o/\sigma(F_o) > 4$ (%)	10.0	10.1	8.8
R_{free} (%)	–	–	11.2
rmsd of bond lengths (Å)	0.014	0.015	0.015
rmsd of bond angles (deg)	1.4	1.4	1.4
Esd in coordinates (Å)			
Main chain atoms	0.03	0.03	0.03
All protein atoms	0.04	0.04	0.04

Table 2. Fe-ligand binding geometries. θ_{bend}, bending angle; τ_{tilt}, tilt angle; $\alpha \approx \theta + \tau$; deut, deuteroporphyrin; THF, tetrahydrofuran; dashes indicate data not available. Numbers in parentheses are standard errors of the last digit or digits.

Crystal	Reference	Method	θ_{bend} (deg)	τ_{tilt} (deg)	α (deg)	Fe-C (Å)	C-O (Å)
MbCO	–	X-ray	7.4(1.9)	4.8(0.9)	–	1.73(3)	1.12(3)
MbCO	(*14*)	IR	7	4	–	–	–
MbCO	(*10*)	IR	–	–	<7	–	–
MbCO	(*11*)	IR	–	–	<10	–	–
MbCO	(*12*)	IR	–	–	6.7(9)	–	–
Fe(TPP)(CO)py	(*3, 8*)	X-ray	1(2)	1.4	–	1.77(2)	1.12(2)
Fe(deut)(CO)(THF)	(*4, 8*)	X-ray	1.7(1.4)	2.5	–	1.706(5)	1.144(5)

comparable occupancy. The imidazole ring of the other conformer (His^{64}-II) is displaced by 0.58 Å in the direction of the protein surface, where it interacts with a partly occupied water, W303 (at 2.53 Å from Nδ_1), in the solvent region. An alternate water site, W302 (at 1.7 Å from W303), can only be populated when the His swings to the His^{64}-I site. The heterogeneity in the solvent environment may explain why the nearby Arg^{45} (CD3) adopts two alternate side-chain conformations in deoxyMb, whereas both Arg^{45} and His^{64} occupy single sites in MbCO. The displacement of the deoxy water has been suggested as providing a substantial barrier to CO binding (*24*), but the deoxy water may leave and reenter the heme pocket even in the absence of CO, which suggests a minor effect of its displacement on the rate constant for CO binding.

Our structural studies indicate that CO binding to Mb is inhibited through a steric hindrance that arises from the orientation of the heme in relation to the E and F helices, which form a topological domain. The ligand may bind only after reorientational motions of the heme and the two helices. These conformational changes represent the most striking structural differences between Mb and CO porphyrin compounds. Concerted rigid-body motions of helices E and F appear to be associated with CO-ligand binding to other heme proteins as well. Raman spectroscopic studies (*25*) provided evidence for a scissorlike motion of the E and F helices in hemoglobin (Hb) after laser-pulse photolysis of HbCO. The α and β subunits (four total) of Hb each have closely similar tertiary structures as Mb; the motions of the helices may transmit a change in heme ligation to the subunit interface (*25*). The ligand-induced motions of the heme and the dynamical domain of the protein matrix, which occur under physiological conditions in Mb and probably also in Hb subunits, are highly correlated and interact synergically. In theory, it should be possible to further study these motions by time-resolved protein crystallography (*26*), provided that a very high resolution can be reached. The displacement of the highly flexible His side chain can only be a minor part of the steric mechanism inhibiting CO binding to heme proteins at ambient temperatures. However, the control of the translocation of the ligand between the docking sites and the active binding site by the swinging motion of the imidazole is probably the main mechanism at low temperature, where the long-range collective movements are suppressed. The structural basis of the discrimination between CO and O_2 under physiological conditions remains uncertain in the absence of an O_2-ligated myoglobin structure at a comparably high resolution. One contribution to a higher affinity of the protein for O_2 may be due to a strong H bond between the O_2 ligand and His^{64} Nε_2 (*1*). Our results suggest that a difference in the Fe-ligand binding geometry may play an important role. If the Fe-O-O unit in heme proteins adopts a similar bent geometry as in oxy porphyrin compounds (*27*), the binding of the O_2 ligand may be expected to involve substantially smaller motions of the heme and the globin than those required for the formation of the near-to-linear Fe-CO bond.

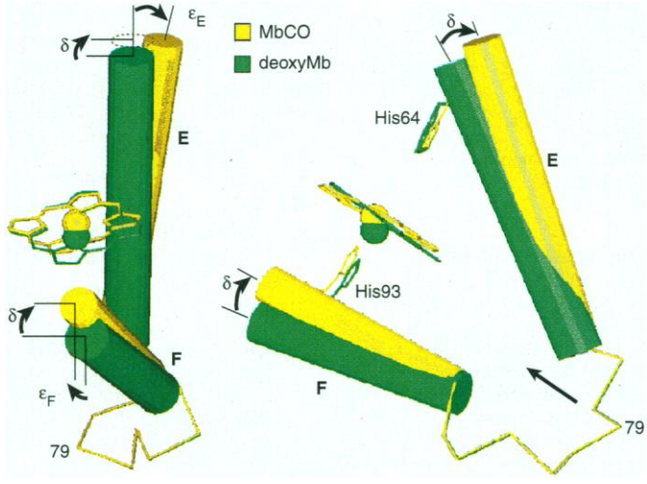

Fig. 2. Schematic view of the motions of the heme, the Fe, and helices E and F, which are required for CO binding to Mb at ambient temperature. δ, joint rotation of E, F, and the Fe; ε_F, joint rotation of F, the heme, and the Fe; and ε_E, rotation of E.

Table 3. Heme geometries. Dashes indicate data not available.

Parameter	MbCO	deoxyMb	Fe(TPP)(CO)py (3)
rmsd of N_4 from plane (Å)	0.006	0.018	–
Fe ··· N_4 plane (Å)*	+0.015	−0.290	–
Average Fe ··· N_4 (Å)	2.005	2.057	2.017
Tilt of pyrrole ring (deg)†			
A	2.4	5.1	2.6
B	0.6	5.5	0.6
C	8.9	12.4	4.4
D	3.5	5.0	3.6

*Positive sign for displacement to the distal side and negative sign for displacement to the proximal side of the N_4 plane.
†Tilt angles between the pyrrole rings and the N_4 plane.

References and Notes

1. B. A. Springer *et al.*, *Chem. Rev.* **94**, 699 (1994).
2. M. Suematsu, Y. Wakabayashi, Y. Ishimura, *Cardiovasc. Res.* **32**, 679 (1996); A. Glabe *et al.*, *Am. J. Physiol.* **274**, H2143 (1998).
3. S.-M. Peng and J. A. Ibers, *J. Am. Chem. Soc.* **98**, 8032 (1976).
4. W. R. Scheidt *et al.*, *Biochemistry* **20**, 3653 (1981).
5. J. Kuriyan *et al.*, *J. Mol. Biol.* **192**, 133 (1986); X. Cheng and B. P. Schoenborn, *ibid.* **220**, 381 (1991).
6. J. P. Collman *et al.*, *Proc. Natl. Acad. Sci. U.S.A.* **73**, 3333 (1976); D. A. Case and M. Karplus, *J. Mol. Biol.* **123**, 697 (1978).
7. J. C. Maxwell and W. S. Caughey, *Biochemistry* **15**, 388 (1976); E. Oldfield *et al.*, *J. Am. Chem. Soc.* **113**, 7537 (1991); B. Kushkuley and S. S. Stavrov, *Biophys. J.* **72**, 899 (1997).
8. G. B. Ray *et al.*, *J. Am. Chem. Soc.* **116**, 162 (1994).
9. P. Jewsbury *et al.*, *ibid.*, p. 11586.
10. M. Lim, T. A. Jackson, P. A. Anfinrud, *Science* **269**, 962 (1995).
11. D. Ivanov *et al.*, *J. Am. Chem. Soc.* **116**, 4139 (1994).
12. J. T. Sage and W. Jee, *J. Mol. Biol.* **274**, 21 (1997); J. T. Sage, *Appl. Spectrosc.* **51**, 568 (1997).
13. S. Hu *et al.*, *J. Am. Chem. Soc.* **116**, 11187 (1994).
14. M. T. McMahon *et al.*, *ibid.* **120**, 4784 (1998).
15. T. Takano, *J. Mol. Biol.* **110**, 569 (1977).
16. A previously reported crystal structure of MbCO at low pH showed an open distal pocket from which the His^{64} side chain has swung out into the solvent [F. Yang and G. N. Phillips Jr., *J. Mol. Biol.* **256**, 762 (1996); M. L. Quillin *et al.*, *Biophys. J.* **61**, A466 (1992)].
17. P. Jewsbury and T. Kitagawa, *Biophys. J.* **67**, 2236 (1994).
18. F. A. Cotton and R. M. Wing, *Inorg. Chem.* **4**, 314 (1965).
19. I. Schlichting *et al.*, *Nature* **371**, 808 (1994).
20. T. Y. Teng *et al.*, *Nature Struct. Biol.* **1**, 701 (1994).
21. H. Hartmann *et al.*, *Proc. Natl. Acad. Sci. U.S.A.* **93**, 7013 (1996).
22. M. Lim *et al.*, *Nature Struct. Biol.* **4**, 209 (1997).
23. D. Vitkup *et al.*, *ibid.*, p. 202.
24. T. Li *et al.*, *Biochemistry* **33**, 1433 (1994).
25. K. R. Rodgers and T. G. Spiro, *Science* **265**, 1697 (1994).
26. V. Šrajer *et al.*, *ibid.* **274**, 1726 (1996).
27. G. B. Jameson *et al.*, *J. Am. Chem. Soc.* **102**, 3224 (1980); J. P. Collman *et al.*, *ibid.* **119**, 3481 (1997).
28. Z. Otwinowski and W. Minor, *Macromolecular Crystallography, Part A*, vol. 276 of *Methods in Enzymology*, C. W. Carter Jr. and R. M. Sweet, Eds. (Academic Press, San Diego, CA, 1997), pp. 307–326.
29. G. W. Sheldrick, SHELXL-97, Göttingen University, Göttingen, Germany (1997); available at http://shelx.uni-ac.gwdg.de/SHELX/
30. D. W. J. Cruickshank, *Acta Crystallogr.* **D55**, 583 (1999).
31. T. A. Jones *et al.*, *ibid.* **A47**, 110 (1991).
32. A. Roussel and C. Cambilleau, TURBO FRODO, Biographics, Centre National de la Recherche Scientifique, Marseille, France (1992).
33. Coordinates and observed structure factors have been deposited in the Protein Data Bank with identification codes 1BZR (MbCO), 1BZP (deoxyMb), and 1BZ6 (metMb).

19 January 1999; accepted 16 March 1999